Synthesis of yttria-doped strontium-zirconium oxide powders via ammonium glycolate combustion methods as precursors for dense ceramic membranes

E. C. LU, E. IGLESIA*
Department of Chemical Engineering, University of California at Berkeley, Berkeley, CA 94720, USA; Materials Sciences Division, E.O. Lawrence Berkeley National Laboratory, Berkeley, CA 94720, USA
E-mail: iglesia@cchem.berkeley.edu

Ammonium glycolate combustion was used to synthesize $SrZr_{0.95}Y_{0.05}O_{3-x}$ powders. Soluble metal-glycolate complexes, detected by infrared spectroscopy, were formed with Y^{+3} and Zr^{+4}, which maintain atomic level mixing of metal cations with glycolic acid. Sr^{+2}/glycolic acid mixtures did not form glycolate complexes. Temperature-programmed reaction studies showed that only precursor solutions with metal-glycolate complexes combust, indicating that the combustion is initiated by metal-glycolate complexes. Varying the ammonium hydroxide content and glycolic acid levels above that required to form glycolate complexes did not affect surface area and crystallinity. Decreasing the glycolic acid/nitrate ratio increases the temperatures reached during combustion. Thick disks prepared from co-precipitated and ammonium glycolate powders demonstrated that combustion synthesized powders reach higher densities. Surface area and SEM indicated that the ammonium glycolate powders have smaller particle sizes, which favor densification, than co-precipitated powders. © *2001 Kluwer Academic Publishers*

1. Introduction

Strontium zirconium yttrium oxide, $SrZr_{1-x}Y_xO_{3-x/2}$, forms crystallites with perovskite structure, which selectively transport protons and oxygen anions [1, 2]. This material and others with similar structure are currently being studied as potential solid oxide electrolytes for fuel cells [2, 3], hydrogen sensors [4], and hydrogen-selective membranes [5–7]. Thick disks are typically synthesized from low surface area ($\sim$1 m²/g) $SrZr_{1-x}Y_xO_{3-x/2}$ powders prepared by co-precipitation or physical mixing. The formation of thin solid oxide electrolytes and membranes is controlled by the particle characteristics of these powders. Powders with more favorable sintering characteristics (e.g. smaller particle sizes) densify to higher fractional densities at lower sintering temperatures [8], leading to thinner $SrZr_{1-x}Y_xO_{3-x/2}$ structures with higher ion transport rates.

Combustion synthesis methods were first reported by Pechini [9] and by Courty and Delmon [10] who showed that mixtures of aqueous metal salts and alpha-hydroxycarboxylic acids formed solid amorphous resins during water evaporation. The organic component of the resin decomposed to form high surface area inorganic powders when treated at higher temperatures ($\sim$873 K). Chick *et al.* [11] reported that heating aqueous metal nitrate-glycine mixtures to $\sim$453 K led to self-sustaining combustion and to the formation of a powder with higher surface area, greater compositional uniformity, and smaller particle sizes than those prepared by the Pechini method. The glycine nitrate process yields high surface area powders by forming metal-organic chelate structures, which prevent the precipitation of cations that would otherwise occur during heating of aqueous metal nitrates [11]. High local temperatures are reached during combustion ($>$1200 K), leading to the formation of crystalline powders. Several groups have shown that combustion synthesis methods, such as glycine nitrate, lead to uniform composition and structure for a wide range of inorganic oxides, $La(Sr)CrO_3$ [11–13], $YBa_2Cu_3O_{7-x}$ [14], calcium aluminates [15], and ZrO_2 [16].

Ammonium glycolate combustion methods are related to the hydroxycarboxylic acid methods [10]. They involve the heating of metal nitrates, glycolic acid, and NH_4OH mixtures to form powders similar to those reported for the glycine-nitrate process, but with less intense and more controllable combustion. This paper reports the study of ammonium glycolate combustion with the aim to understand the details of the combustion synthesis pathways. This study includes an analysis of complexes formed in the precursor solution, the

---

* Author to whom all correspondence should be addressed.

effect of precursor solution composition on the combustion and the characteristics of $SrZr_{1-x}Y_xO_{3-x/2}$ powders, where $x = 0.05$. A comparison between ammonium glycolate and co-precipitated powders on their ability to form dense disks and films with orthorhombic perovskite structure is also presented.

2. Experimental
2.1. Synthesis of powders and disks
In the ammonium glycolate method, $Sr(NO_3)_2$, $Y(NO_3)_3$, and $ZrO(NO_3)_2$ solutions (1.35 M, 1.14 M, and 0.323 M, respectively, analyzed by inductively coupled plasma optical emission spectroscopy, ICP-OES) were prepared from nitrate salts (Aldrich, Inc., 99% purity). An aqueous mixture of metal nitrates with the stoichiometry of the $SrZr_{0.95}Y_{0.05}O_{3-x}$ phase and glycolic acid (GA) [GA/(Sr + Y + Zr) molar ratio of 3] was prepared. The (GA)/nitrate molar ratio was then adjusted using 15.8 N HNO_3; concentrated ammonium hydroxide (NH_4OH, 14.8 N) was then added to obtain a pH of 8. The total amount of solution used varied from 1 cm^3 (in a 50 cm^3 beaker) to 550 cm^3 (in a 2000 cm^3 beaker) with theoretical yields of $SrZr_{0.95}Y_{0.05}O_{3-x}$ of 0.5 g to 31 g, respectively. The beaker containing the precursor solution was covered with a stainless steel wire screen (100-mesh) in order to prevent powder loss and placed within an open-top metal box as a safety precaution. The clear solution was heated without mixing using a heating lamp (250 W) placed ~2 cm below the bottom of the beaker. The resulting powder was crushed with a mortar and pestle, and then treated in air at 0.167 K/s to 1273 K for 4 h in order to decompose any organic residues. ICP-OES analysis showed that the synthesized powders had the correct stoichiometry.

In the co-precipitation method, a stoichiometric mixture of the same metal nitrate solutions and a 2 M $(NH_4)_2CO_3$ (>99.9% pure, Fisher Scientific) solution were prepared. The metal nitrate solution was added dropwise (0.08–1.67 cm^3/s) to the $(NH_4)_2CO_3$ solution as the latter was mixed with an impeller, and a 2.5 M NH_4OH solution was added to maintain the pH at 9. Carbonate anions are required in order to precipitate strontium as $SrCO_3$ because $Sr(OH)_2$ is soluble in water at all pH values. Solutions were metered by pumps (Masterflex model 7518-60) and the pH was measured using a meter (OMEGA pHB-62). The resulting precipitate consisted of Zr and Y hydroxides and Sr carbonates. It was filtered using a Buchner funnel (Whatman #40 filter paper) and dried overnight in air at 400 K. The powder was then treated in air at 0.167 K/s to 1373 K for 4 h in order to form the perovskite phase.

$SrZr_{0.95}Y_{0.05}O_{3-x}$ powders (1.0 g) prepared by the two methods were pressed in a 25 mm diameter die at ~180 MPa to form cylindrical disks (~1 mm thick). Disks were sintered at a rate of 0.167 K/s to 1873 K, held for 4 h, and cooled at 0.167 K/s in flowing dry air (1.67 cm^3/s).

2.2. Characterization methods
Aqueous complexes formed by Sr^{+2}, Y^{+3}, and Zr^{+4} with glycolic acid were detected using infrared spectroscopy (Mattson RS-10000 spectrometer) and a cell equipped with BaF_2 windows. Competing ligand titration experiments [17] were performed in order to determine the number of glycolate ligands in the soluble glycolate complexes. Aqueous metal nitrates were titrated into a 10 cm^3 aqueous solution of 0.1–0.3 g glycolic acid maintained at a pH of 9 with NaOH or NH_4OH. The titration endpoint is reached when all the glycolic acid is complexed with the metal cations; it was detected by the incipient precipitation of metal hydroxides.

Temperature-programmed synthesis reaction studies were performed by continuous analysis of the gases evolved during combustion using a mass spectrometer (Leybold Inficon Transpector RCA-200) and by syringe sampling (5890 series II Hewlett Packard gas chromatograph/mass spectrometer, HP-1 crosslinked methyl siloxane column, 50 m × 0.32 mm) during combustion. A 0.40 cm^3 sample of the precursor solution was placed within a quartz reactor, the temperature was ramped at 0.17 K/s to 473 K and at 0.03 K/s above 473 K, and the carrier gas was metered by mass flow controllers (Porter Instruments). The flowing gases (1.67 cm^3/s) consisted of varying amounts of O_2 (0–20%) in a 3% Ar/He carrier gas (Praxair, UHP).

Powder X-ray diffraction patterns were obtained using a diffractometer (Siemens D5000) with Cu K_α radiation ($\lambda = 1.5406$ Å). Surface areas were obtained from N_2 physisorption at its boiling point using an Autosorb-6 automated surface area analyzer (Quantachrome, Inc.) after removing adsorbed water from samples at 383 K for 2 h under vacuum. Electron microscopy was performed on a dual-stage ISI-DS130C scanning electron microscope (SEM). Powder samples were coated in a Au sputterer for 120 s at 40 mA in order to increase the conductivity.

The extent of densification of $SrZr_{0.95}Y_{0.05}O_{3-x}$ disks was measured by their fractional density (measured density/skeletal density of $SrZrO_3$, 5.46 g/cm^3). The dimensions were measured using microcalipers and the weight was determined using a 4-digit microbalance (Denver Instruments M-220).

3. Results and discussion
3.1. Precursor solution analysis
Fig. 1 shows the infrared spectra of an aqueous glycolic acid solution at pH values of 2, 9 (by adding NH_4OH), and 11 (by adding NaOH). In each sample, a broad water band was detected between 1550–1750 cm^{-1}. The spectral noise at frequencies between 1400–1800 cm^{-1} arises from water vapor. The symmetric and asymmetric stretches of the carboxylate group at ~1600 cm^{-1} and 1400 cm^{-1}, respectively, were not visible. The C-O stretching frequency and the in-plane bending frequency of the C-OH group were visible at 1095 cm^{-1} and 1250 cm^{-1}, respectively, only for the low pH solution. The assignment of these bands is consistent with a normal coordinate analysis of the glycolic acid spectra reported by Nakamoto, *et al.* [18]. The in-plane bending band shifts from 1250 to 1329 cm^{-1} and the C-O stretching band shifts from 1095 to 1078 cm^{-1} when the pH is increased with NH_4OH or NaOH.
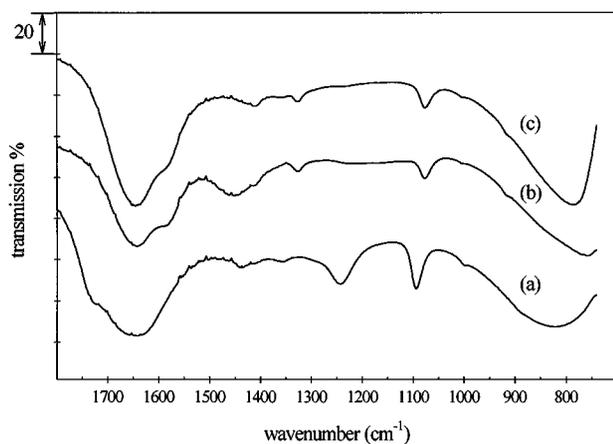
Figure 1 Infrared spectra of glycolic acid (a) 1.02 M glycolic acid pH = 2 (b) 1.02 M glycolic acid + NH$_4$OH, pH = 9 (c) 1.02 M glycolic acid + NaOH, pH = 11.

Figure 3 Infrared spectra of Y complexes (a) 1.14 M Y(NO$_3$)$_3$ + NH$_4$OH w/GA/MC = 3, pH = 7 (b) 1.14 M Y(NO$_3$)$_3$ + NH$_4$OH w/GA/MC = 4, pH = 7.

Both shifts are attributed to the dissociation of the carboxylic acid group in glycolic acid at pH values above 4 (pKa = 3.83).

$$HOCH_2COOH + H_2O \underset{\rightarrow}{\leftarrow} HOCH_2COO^- + H_3O^+ \quad (1)$$

The in-plane bending band shifts to higher wavenumbers because hydrogen bonding between the carboxylic and the alcohol groups becomes stronger as the negative charge of the glycolate anion increases [19]. The negative charge of the carboxylic group also reduces the polarity in the C^+-O^- bond of the alcohol group, weakening it and decreasing the C-O stretching frequency [20].

Infrared spectra showed that Sr^{+2} did not form glycolate complexes at (GA)/metal molar ratios between 1 and 2 and pH values between 3 and 11 (Fig. 2). Gas phase water (1400–1800 cm^{-1}), liquid water (1600–1700 cm^{-1}), and nitrate (1350–1500 cm^{-1}) infrared absorption bands obscured any spectral features above 1300 cm^{-1}. The in-plane bending (1250 cm^{-1}) and stretching (1095 cm^{-1}) frequencies of the C-OH group of glycolic acid in mixtures of Sr(NO$_3$)$_2$ and glycolic acid (at pH = 3) were identical to those observed for pure glycolic acid. The in-plane bending band at 1250 cm^{-1} disappeared and the C-O stretching band shifted from 1095 cm^{-1} to 1078 cm^{-1} when the pH was increased to 8 by adding NH$_4$OH or NaOH (not shown). The in-plane bending band probably shifted to 1329 cm^{-1}, as it did for pure glycolic acid, but it is masked by the strong absorption bands of the nitrate groups. The similarity between these spectra and that of pure glycolic acid suggests that Sr^{+2} does not form glycolate complexes because the C-OH bands did not shift as expected when glycolic acid complexes with Sr^{+2}.

The shift of in-plane bending of C-OH bonds in glycolic acid/Y(NO$_3$)$_3$ mixtures shows that Y^{+3} formed aqueous glycolate complexes at (GA)/metal ratios above 3 and pH values between 5 and 7. Precipitation occurred at (GA)/metal ratios between 1 and 4 at pH values below 4 and it also was observed for solutions with (GA)/metal ratios below 3 at pH values above 4. Aqueous solutions of Y(NO$_3$)$_3$ and of Y(NO$_3$)$_3$/(GA) corroded the BaF$_2$ windows and their spectra could not be measured. Fig. 3 shows the infrared spectra of Y(NO$_3$)$_3$/(GA) mixtures at a pH of 7. The in-plane bending band of the C-OH group of glycolic acid appeared at 1111 cm^{-1} but the C-O stretch remained at 1078 cm^{-1}. The shift of the in-plane bending band of the C-OH group reflects a decrease in the strength of hydrogen bonding between the H in the C-OH group and the carboxylate group as glycolic acid forms complexes with Y^{+3} via the carboxylate group. If a chelate had formed, the C-O stretching band would have shifted to lower wavenumbers, because the C-O bond is weakened by direct metal cation-oxygen bonds using oxygen atom in the C-OH group [20]. Schematic diagrams of chelate complexes and carboxylate complexes are shown in Fig. 4. The low intensity in the water (1650 cm^{-1}) and in the nitrate (1400 cm^{-1}) frequency regions is caused by total light absorption by these solutions.

The spectra shown in Fig. 5 suggest that Zr^{+4} also forms glycolate complexes via the carboxylate group at (GA)/metal molar ratios above 2 and pH values between 5 and 11. The addition of glycolic acid to ZrO(NO$_3$)$_2$ led to white amorphous precipitates at (GA)/metal

Figure 2 Infrared spectra of Sr complexes (a) 1.35 M Sr(NO$_3$)$_2$, pH = 3 (b) 1.35 M Sr(NO$_3$)$_2$ w/GA/MC = 1.0, pH = 3 (c) 1.35 M Sr(NO$_3$)$_2$ + NH$_4$OH w/GA/MC = 1.0, pH = 8 (d) 1.35 M Sr(NO$_3$)$_2$ + NH$_4$OH w/GA/MC = 2, pH = 8.
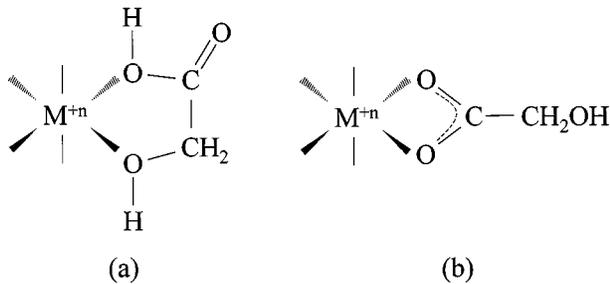
Figure 4 Schematic pictures of (a) insoluble chelate complexes and (b) soluble glycolate complexes.
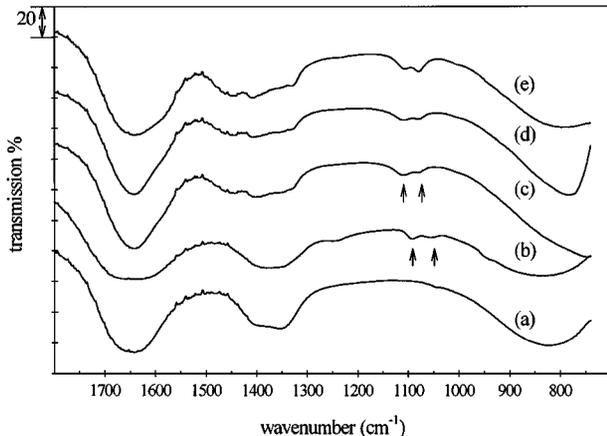
Figure 5 Infrared spectra of Zr complexes (a) 0.323 M $ZrO(NO_3)_2$, pH $= 0.7$ (b) 0.323 M $ZrO(NO_3)_2$ w/GA/MC $= 2$, pH $= 0.5$ (c) 0.323 M $ZrO(NO_3)_2 + NH_4OH$ w/GA/MC $= 2$, pH $= 11$ (d) 0.323 M $ZrO(NO_3)_2 + NH_4OH$ w/GA/MC $= 3$, pH $= 11$ (e) 0.323 M $ZrO(NO_3)_2 + NH_4OH$ w/GA/MC $= 4$, pH $= 11$.

ratios between 1 and 4 and pH values below 4. These precipitates dissolved when the (GA)/metal ratios increased above 2 for pH values above 5. Infrared spectra of the precipitates show the in-plane bending band at 1250 cm^{-1}, the C-O stretch at 1095 cm^{-1}, and a new band at 1058 cm^{-1}. The band at 1058 cm^{-1} is attributed to a shift of the C-O stretching band indicating the formation of an insoluble glycolate chelate [20]. The spectra of precipitate-free solutions at pH values above 5 showed that in-plane bending bands shifted to 1111 cm^{-1} and the C-O stretch appears at 1078 cm^{-1}, suggesting that the soluble Zr glycolate complex bonds via the carboxylate group as it had for Y.

The number of glycolate ligands required to form the soluble glycolate complexes was confirmed by competing ligand titration experiments. The results showed that the moles of glycolic acid per mole of metal required to form soluble glycolate complexes at pH values between 5 and 11 is 3.4 and 1.6 for Y^{+3} and Zr^{+4}, respectively. These values are consistent with infrared spectra that showed that Y^{+3} and Zr^{+4} required approximately three and two moles of glycolic acid per mole of metal, respectively, in order to form the aqueous glycolate complexes. These glycolate complexes exhibit greater solubility at pH values between 5 and 11 than $Y(OH)_3$ and $Zr(OH)_4$, which would precipitate at these pH values in the absence of the glycolic acid required in order to form soluble glycolate complexes. A summary of the solubility observations and results are shown in Table I.

T A B L E I Summary of solubility observations

aqueous metal	glycolic acid/metal molar ratio	pH (base added)	precipitation? (species)
Sr(NO$_3$)	0–2	2–11 (NaOH, NH$_4$OH)	no
Y(NO$_3$)$_3$	0–2	2–7 (NaOH, NH$_4$OH)	no
	0–2	7–11 (NaOH, NH$_4$OH)	yes (hydroxide)
	$\geq$3	2–4 (NaOH, NH$_4$OH)	yes (glycolate)
	$\geq$3	5–11 (NaOH, NH$_4$OH)	no
ZrO(NO$_3$)$_2$	0–1	$\leq$1 (NaOH, NH$_4$OH)	no
	0–1	2–11 (NaOH, NH$_4$OH)	yes (hydroxide)
	$\geq$2	2–4 (NaOH, NH$_4$OH)	yes (glycolate)
	$\geq$2	5–11 (NaOH, NH$_4$OH)	no

The formation of individual soluble metal glycolate complexes maintains atomic level mixing between metal cations and glycolic acid, leading to metal-initiated combustion and to concurrent nucleation of metal cations. Mixtures of aqueous $Y(NO_3)_3$ or $ZrO(NO_3)_2$ with glycolic acid led to amorphous white precipitates at pH values below 4 (molar ratios GA/Zr, GA/Y $= 1$–4) and to clear solutions when the pH was raised to 5–11 by adding NH_4OH or $NaOH$ (molar ratios GA/Zr $= 2$–4, GA/Y $= 3$–4). The precipitates formed at pH values below 4 and the soluble complex detected at pH values above 4 were shown to be glycolate species by infrared measurements. In addition, the soluble species at higher pH values are not ammonium complexes, because the substitution of NaOH for NH$_4$OH led to similar solubility behavior and infrared spectra. These results suggest that the following solution equilibria govern the behavior of these mixtures.

$$M^{+n} + x HOCH_2COOH + n OH^- \overset{\rightarrow}{\leftarrow}$$
$$[M(HO\text{-}CH_2\text{-}COOH)_x(OH)_n]_{(s)} \qquad (2)$$
$$HOCH_2COOH + H_2O \overset{\rightarrow}{\leftarrow} HOCH_2COO^- + H_3O^+ \qquad (3)$$
$$M^{+n} + n HOCH_2COO^- \overset{\rightarrow}{\leftarrow} M(HOCH_2COO)_{n(aq)} \qquad (4)$$
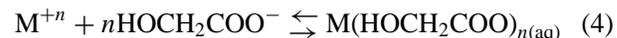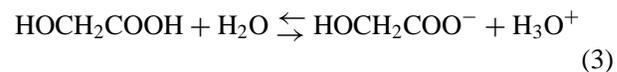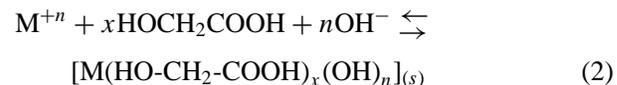
where M^{+n} stands for Y^{+3} and ZrO^{+2}, respectively. These equations describe how precipitation of metal-glycolate species occurs at low pH values, for which glycolic acid exists primarily in the protonated form. It also shows that increasing the pH shifts the equilibrium of glycolic acid hydrolysis (Equation 2) to the right, so that glycolic acid exists as an ionized species and the soluble glycolate complex forms via reaction with solvated cations. The chelate has lower solubility than the glycolate because the hydroxyl group is bonded to the metal cation (Fig. 4), thus reducing the hydrogen bonding that occurs between the complex and the water solvent.

3.2. Characterization of combustion processes

Fig. 6 shows the change in molar flow rate for precursor solutions with varying (GA)/nitrate ratios during

solution composition	GA/ metal	GA/ nitrate	pH	gas phase	combustion?	extent of combustion (*)
GA	N/A	N/A	8	20% O_2	no	0.0
GA, HNO_3	N/A	1.0	8	20% O_2	no	0.0
Sr, GA	2	1.0	8	20% O_2	no	0.0
Y, GA	3	1.0	8	20% O_2	yes	—
Zr, GA	2	1.0	8	20% O_2	yes	—
Sr, Zr, Y, GA	2	1.0	8	20% O_2	yes	—
"	3	1.0	8	20% O_2	yes	1.7
"	4	1.0	8	20% O_2	yes	1.5
"	3	1.0	2	20% O_2	no	0.0
"	3	1.0	5	20% O_2	yes	1.5
"	3	1.5	8	20% O_2	yes	<0.01
"	3	0.5	8	20% O_2	yes	1.5
"	3	1.5	8	inert	no	0.0
"	3	1.0	8	inert	no	0.0
"	3	0.5	8	inert	yes	0.6

GA – glycolic acid.
Sr – 1.4 M $Sr(NO_3)_2$.
Y – 1.1 M $Y(NO_3)_3$.
Zr – 0.3 M $ZrO(NO_3)_2$.
* – moles of gas evolved per mole of glycolic acid.
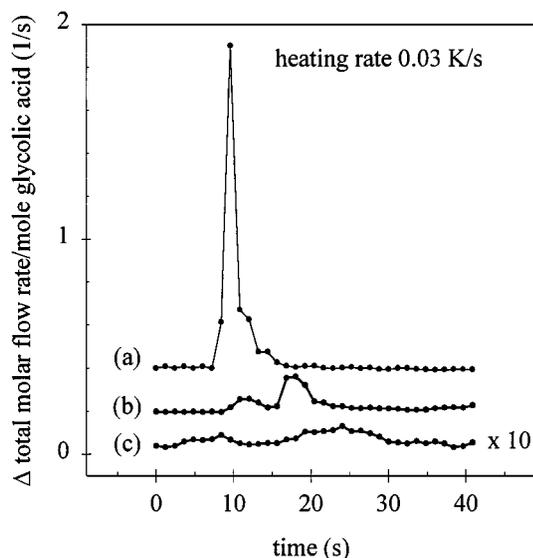
Figure 6 Volume expansion measured during temperature-programmed reaction experiments, (GA)/nitrate = (a) 0.5 (b) 1.0 (c) 1.5.

temperature-programmed synthesis. (GA)/nitrate ratios of 0.5 led to the most rapid combustion. Increasing this ratio led to slower combustion. Table II shows the results of temperature-programmed reaction studies using different precursor solutions and gas phase compositions. Combustion was detected by a rapid drop in the internal standard (Ar) concentration. The extent of combustion was defined as the total moles of gas evolved, determined by integrating the change in molar flow rate, divided by the amount of glycolic acid in solution.

The absence of combustion in solutions of glycolic acid, (GA)/HNO_3, or $Sr(NO_3)_2$/(GA), and the combustion detected for $Y(NO_3)_3$/(GA) and $ZrO(NO_3)_2$/(GA) mixtures confirm that combustion is initiated by metal-glycolate complexes. The first three solution compositions did not contain metal-organic bonds, while the

latter two solutions formed glycolate complexes. The precursor solution without NH_4OH (at a pH of 2) did not combust because Y and Zr glycolate complexes precipitated before heating. Kingsley and Pederson [21] found that the ignition temperature depends on which metal cations exist as complexes in glycine nitrate processes; this also suggests that the combustion is metal initiated.

These data also show that combustion depends on the amount of local oxidant available in the solution and in the gas phase. The extent of combustion decreased dramatically to <0.01 moles of gas/GA mole for (GA)/nitrate ratios of 1.5 compared to 1.7 and 1.5 moles/GA mole for the (GA)/nitrate ratios of 1.0 and 0.5, respectively. No O_2 consumption was detected during any of these experiments, (MS detection limit 0.01% conversion). Removing O_2 from the gas phase prevented combustion for solutions of (GA)/nitrate ratios of 1.5 and 1.0, but not for (GA)/nitrate ratios of 0.5. The differences observed with and without O_2 showed that O_2 was required for fuel-rich (GA)/nitrate ratios. The low O_2 conversions and its dependence on (GA)/nitrate ratios, however, suggest that, once initiated, combustion relies upon the local source of oxidants (nitrates). Therefore, the stoichiometric reaction (Equation 5) for complete combustion of glycolic acid, $Sr(NO_3)_2$, and $ZrO(NO_3)_2$ to N_2, CO_2, and H_2O is:

$$6C_2H_4O_3 + Sr(NO_3)_2 + ZrO(NO_3)_2 + 3.2HNO_3$$
$$\rightarrow SrZrO_3 + 3.6N_2 + 12CO_2 + 13.6H_2O \quad (5)$$
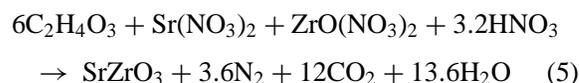
$Y(NO_3)_3$ and NH_4OH are excluded from the combustion equation because $Y(NO_3)_3$ is in relatively small quantities and NH_4OH did not influence the temperature-programmed reaction results. This equation shows that the stoichiometric (GA)/nitrate ratio required for complete combustion is 0.83 and that the reaction should produce 4.83 moles of gas/GA mole. A (GA)/nitrate ratio of 1.5 corresponds to a fuel-rich mixture and it does not contain sufficient nitrate groups to oxidize all glycolic acid; therefore, such mixtures lead to low extents of combustion. The fuel-lean mixture ((GA)/nitrate ratio of 0.5) has enough oxidant to combust the glycolic acid, and such mixtures lead to higher extents of combustion. The similarity between the fuel-lean and stoichiometric extents of combustion suggests that excess nitrate does not inhibit combustion. Fuel-lean mixtures, however, will be shown in later sections to reach higher local reaction temperatures during combustion than stoichiometric or fuel-rich mixtures. The extent of combustion measured for those that combusted corresponded to 31–35% of the value expected for complete combustion. These low values are attributed to incomplete combustion and to the formation of oxygen-containing organics (i.e. CH_2O_3) and CO, which were detected in the combustion effluent by GC/MS. These products formed because combustion propagates like a wave through the precursor solution where high local temperatures are unable to be maintained for sufficient time to ensure complete combustion to CO_2, leading to the formation of the oxygen containing organics.

treatment temperature (K)	(GA)/metal	(GA)/nitrate	pH	Surface Area (m^2/g)	% wgt loss	crystallite radius (nm)
298	2	1.0	8	13.6	0.0	—
	3	1.0	8	13.4	0.0	—
	4	1.0	8	15.9	0.0	—
	3	1.0	5	13.2	0.0	—
553	2	1.0	8	21.2	2.3	—
	3	1.0	8	18.6	3.3	—
	4	1.0	8	23.7	3.1	—
	3	1.0	5	18.3	4.9	—
793	2	1.0	8	23.8	6.4	7.1
	3	1.0	8	27.1	7.8	—
	4	1.0	8	37.1	9.4	8.7
	3	1.0	5	24.2	10.5	8.1
1023	2	1.0	8	27.1	11.8	10.1
	3	1.0	8	26.3	13.3	10.6
	4	1.0	8	29.6	12.1	10.3
	3	1.0	5	27.7	17.2	11.8
1273	2	1.0	8	14.7	14.5	15.1
	3	1.0	8	14.3	16.4	14.7
	4	1.0	8	19.3	15.1	14.9
	3	1.0	5	15.2	20.2	15.3

Figure 7 Evolution of perovskite phase with treatment temperature [GA/MC = 2, GA/NO$_3$ = 1.0, pH = 8, 1.2 g yield].

Figure 8 Surface area changes with treatment temperature and GA/NO$_3$. (a) GA/NO$_3$ = 1.5 (b) GA/NO$_3$ = 1.0 (c) GA/NO$_3$ = 0.5 [GA/MC = 3, pH = 8, 1.2 g yield for all samples].

3.3. Precursor solution composition and temperature treatment effects on powder characteristics

The surface area and the evolution of the perovskite phase were not influenced by the (GA)/metal ratio (2–4) or the pH (5–8) (Table III). The surface area increased with treatment temperature between 553 and 793 K, as the result of the removal of organic residues or non-reacted metal-organic complexes, a process that exposes previously inaccessible surface area or leads to additional formation of powder. These air treatments decrease the weight of the powders formed via glycolate combustion methods. Treatment at higher temperatures (1023–1273 K) sintered the powders and decreased surface areas as a result of sintering. The perovskite phase was not detected by XRD at temperatures below 793 K (Fig. 7). The perovskite phase may exist in samples treated at 553 K, but the crystallites are possibly too small to be detected by diffraction methods (<3 nm). The crystallite size, calculated from the line breadth of the [002] reflection, was not influenced by the glycolic/metal ratio or pH (Table III).

The surface area and diffraction results are independent of the (GA)/metal ratio or the pH over the range examined, consistent with the kinetic measurements of combustion rate and extent. Glycolic acid is required as a fuel for combustion, but glycolic acid amounts beyond those required to complex the metal cations did not influence the extent of combustion. NH$_4$OH does not influence or participate in the combustion, but it increases the pH of the precursor solution in order to maintain the metal cations in solution.

Varying the (GA)/nitrate ratio led to changes in the surface area and crystallinity of the powders formed. Stoichiometric and fuel-rich powders showed similar changes in surface area with treatment temperature. The fuel-lean powder, however, had a lower initial surface area at 298 K than stoichiometric and fuel-rich powders (9 vs. 14 m^2/g); it showed very little increase in surface area between 298–793 K, and then a slight decrease from 793–1273 K (Fig. 8). Thermogravimetric analyses showed that the weight loss after treatment at 1273 K for fuel-rich, stoichiometric, and fuel-lean powders was 4.36%, 16.43%, to 30.20%, respectively, indicating a decrease in the amount of organic residue with decreasing (GA)/nitrate ratio. X-ray diffraction showed that the orthorhombic perovskite phase was detectable at lower treatment temperatures as the (GA)/nitrate ratio was decreased (Figs 7, 9, and 10). The smaller changes in surface area and crystallinity for fuel-lean powders suggest that fuel-lean precursor solutions led
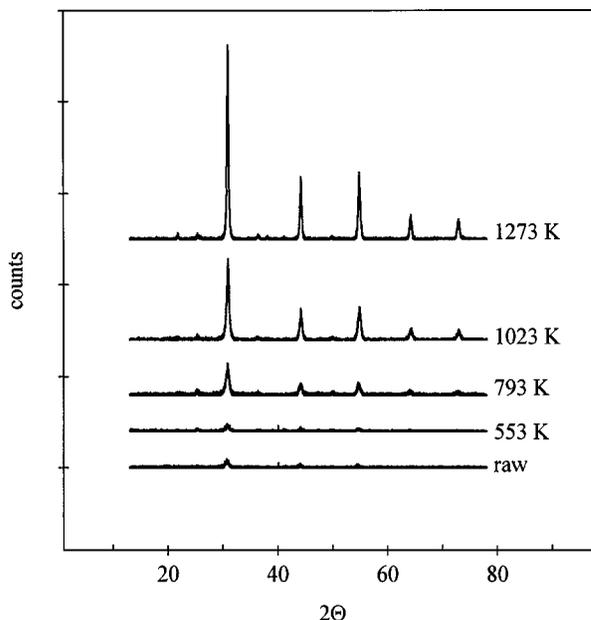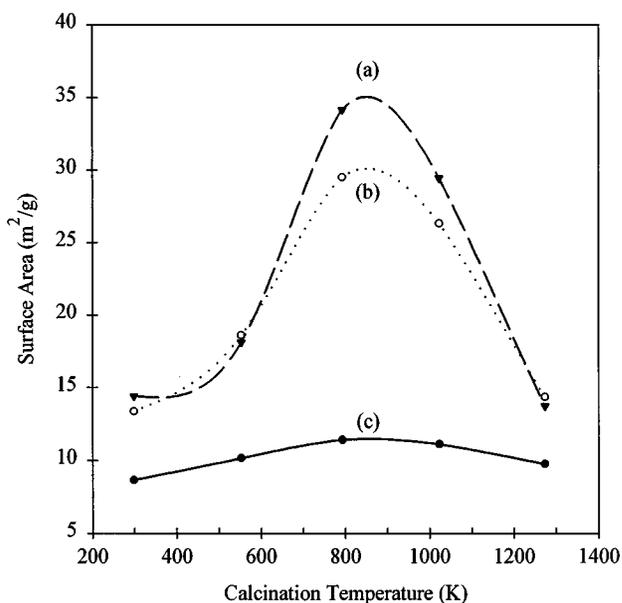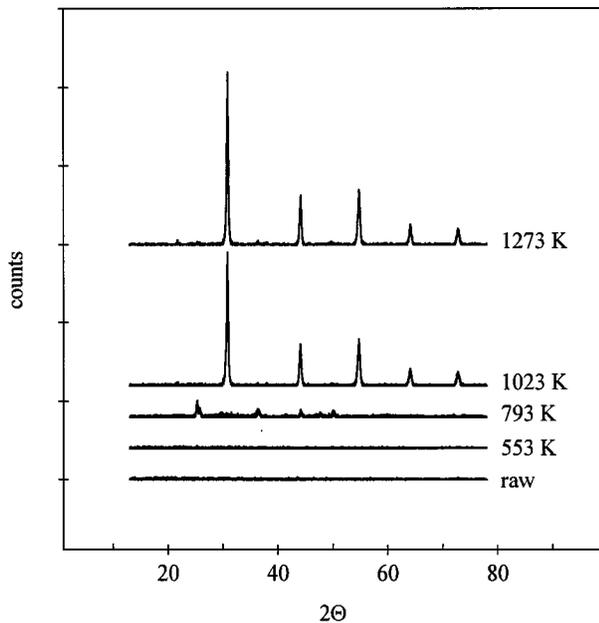
Figure 9 Change in phase with treatment temperature [GA/NO$_3$ = 1.5, GA/MC = 3, pH = 8, 1.2 g yield].
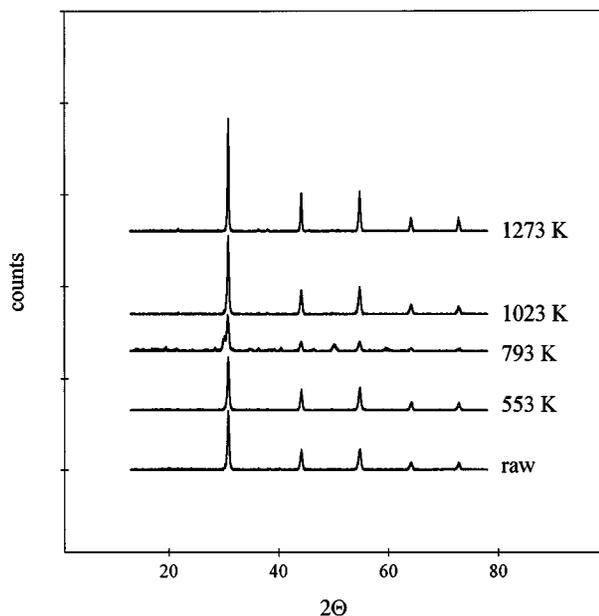
Figure 10 Change in phase with treatment temperature [GA/NO$_3$ = 0.5, GA/MC = 3, pH = 8, 1.2 g yield].

to higher temperatures during combustion than stoichiometric and fuel-rich solutions.

The temperatures measured during combustion by a thermocouple (type K) placed in the precursor solution are consistent with these results. Fuel-rich mixtures showed slightly lower maximum temperatures (~700 K) than stoichiometric mixtures; fuel-lean mixtures reached much higher temperatures (which damaged the thermocouple). The amount of powder produced also depended on the (GA)/nitrate ratio. The fuel-rich solution produced only ~34% of the theoretical powder yield, most likely because of unreacted glycolate complexes that adhered to beaker walls, while the fuel-lean produced ~80%.

Temperature-programmed reaction experiments showed that O$_2$ is not a significant oxidant source for combustion and that nitrates are the predominant oxidant available during rapid (diffusion-limited) reactions. In fuel-rich precursor solutions ((GA)/nitrate = 1.5), nitrates are the limiting reactants, preventing combustion of glycolic acid and leading to regions that cool and extinguish. Increasing the nitrate content (e.g. (GA)/nitrate = 1.0 or 0.5) overcomes this limitation and leads to continuous combustion of glycolic acid and to higher local temperatures.

In our study, fuel-lean precursor solutions led to the highest combustion temperatures. Chick *et al.* concluded instead that precursor solutions with stoichiometric fuel/oxidant ratios led to the highest temperatures in the glycine nitrate process, a similar combustion synthesis method [11]. NH$_4$OH was excluded from the combustion reaction stoichiometry (Equation 5), based on the finding that the presence of NH$_4$OH (used to vary the pH) did not influence the extent of combustion, the surface area, or the crystallinity. If NH$_4$OH, however, were oxidized by nitrates, the reaction stoichiometry would be:

$$6C_2H_4O_3 + Sr(NO_3)_2 + ZrO(NO_3)_2 + 6.2HNO_3$$
$$+ 5NH_4OH \rightarrow SrZrO_3 + 7.6N_2 + 12CO_2$$
$$+ 27.6H_2O \qquad (6)$$
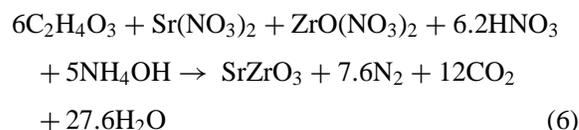
The stoichiometric (GA)/nitrate ratio for this reaction is 0.59 vs. 0.83 for Equation 5 indicating that (GA)/nitrate ratios of 0.5 were approximately stoichiometric if NH$_4$OH was oxidized. Our results would then be consistent with that of Chick *et al.* NH$_4$OH may not affect the combustion because its relative contribution to the combustion is much smaller than that of glycolic acid. It is not conclusive, however, whether Equation 6 represents the overall stoichiometric combustion more accurately than Equation 5.

3.4. Comparison of ammonium glycolate and co-precipitation powders

Thick disks formed from ammonium glycolate powders reached higher fractional densities than those formed from co-precipitated powders. Fig. 11 shows the effect
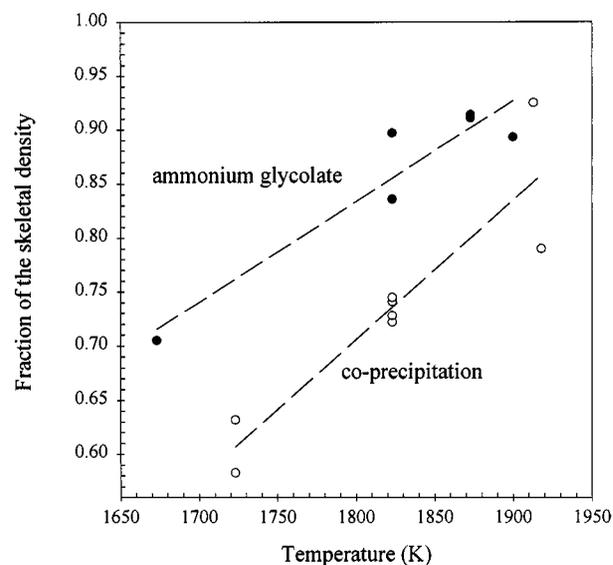
Figure 11 Fraction of the skeletal density vs. sintering temperature.
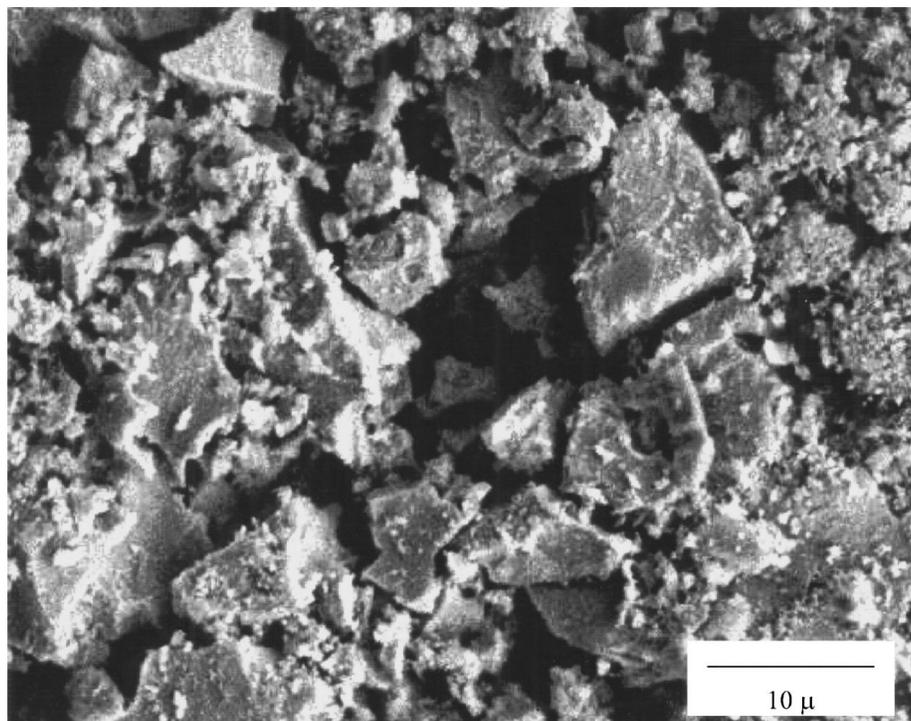
Figure 12 SEM of co-precipitated powders [treated at 1373 K for 4 h in air].

of sintering temperature on the fractional density of thick disks (the initial fractional density was 0.50–0.60 for all disks) prepared by each synthesis method. The ammonium glycolate disks were significantly denser than those formed from co-precipitated powders at all sintering temperatures. Since the disks were prepared identically, the differences in final density most likely reflect differences in the particle characteristics (e.g. particle size) between ammonium glycolate and co-precipitated powders. A particle is defined as a crystallite or collection of crystallites, which can not be reduced physically to smaller sub-units.

The surface area of the ammonium glycolate powder was higher than the co-precipitated powder (14.7 vs. 1.7 m^2/g). Assuming non-porous quasi-spherical particles, the surface area measurements were used to estimate the average particle radii, which were 0.037 μ and 0.323 μ for ammonium glycolate and co-precipitated particles, respectively. Pore radii measurements by N_2 physisorption of ammonium glycolate powder disks before sintering showed that the pore radii between particles was consistent with that for the packing of non-porous spherical particles suggesting that our assumption is valid. SEM also showed that the particle size of co-precipitated powders was larger than that of the ammonium glycolate powders (Figs 12 and 13). The size of the particles in the SEM pictures, however, is larger than that estimated by the surface area for both powders. In the case of the ammonium glycolate powder, the discrepancy between the surface area and SEM results reflects the formation of porous agglomerates. SEM is unable to detect the particle size or the small pores in the agglomerate because they are too small, while N_2 physisorption is able to penetrate the pores and accurately detect the particle size. For co-precipitated powders, the larger particles contribute

insignificantly to the surface area measurements and therefore the estimated particle size represents only the portion of particles in the sub-micron range.

The smaller particle sizes of the ammonium glycolate powders led to higher density disks because the contribution of densification mechanisms during sintering (e.g. bulk diffusion) increases more than coarsening mechanisms (e.g. vapor transport) as the particle size is reduced [8, 22, 23]. The dependence of the rate of these mechanisms on the particle radius, r, was shown to be [22]:

$$\text{rate} \sim r^{-3/5} \quad \text{bulk diffusion}$$
$$\text{rate} \sim r^{-2/3} \quad \text{vapor transport}$$

Disks prepared from ammonium glycolate derived powders were also stronger and maintained their shape indefinitely; in contrast, co-precipitated disks crumbled into powder after about 24 h in ambient air at room temperature. These phenomena appear to reflect the weaker joints formed between particles in disks prepared from co-precipitated powders than those from ammonium glycolate powders. The more porous disks prepared from co-precipitated powders allow CO_2 and H_2O to penetrate the disk, possibly leading to the formation of $SrCO_3$ or other compounds with lower density than $SrZr_{0.95}Y_{0.05}O_{3-x}$ causing disk volume expansion and break up.

The ammonium glycolate and co-precipitation method form particles by nucleating particles under supersaturated conditions [24]. The ammonium glycolate method leads to smaller particles than the co-precipitation method because it is able to rapidly reach local supersaturation and then isolate particles from unreacted precursor by rapid expansion. The co-precipitation method nucleates particles, which remain
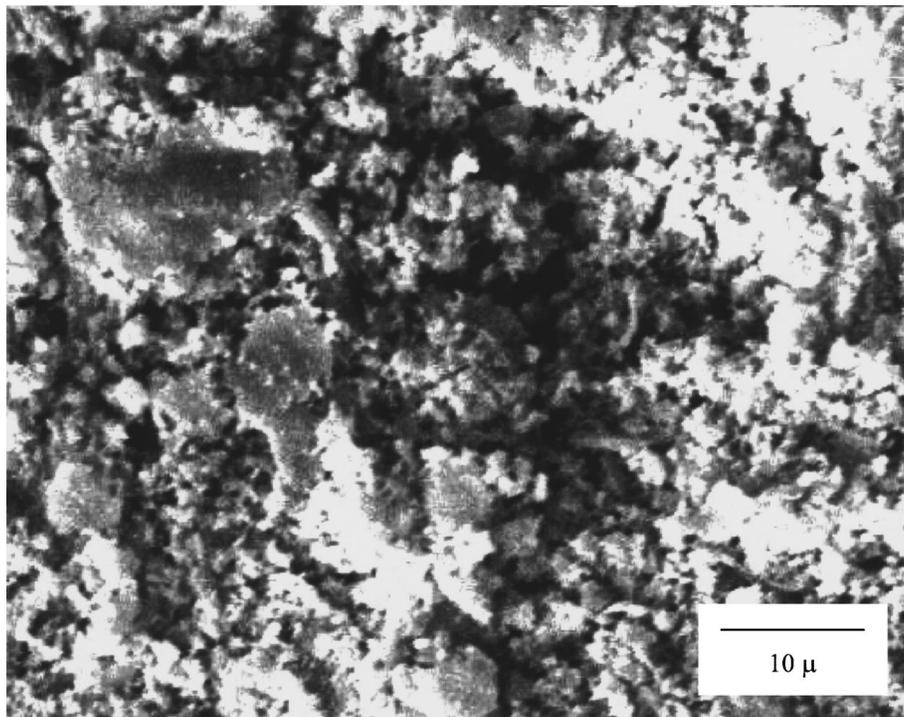
Figure 13 SEM of powders [GA/nitrate = 1.0, GA/metal = 4, pH = 8, treated 1273 K for 4 h in air].

in a solution containing additional reactants, leading to more particle growth and fewer nuclei than in the ammonium glycolate combustion method.

4. Conclusions

Ammonium glycolate combustion pathways begin with the formation of metal-glycolate complexes in the precursor solution, which maintain atomic level mixing at conditions that would otherwise lead to precipitation; they also provide sites for low-temperature metal-initiated combustion. Combustion leads to local supersaturation of metal cations at the combustion front by removing the organic component of the soluble complex and rapidly evaporating water due to the generation of high temperatures. The wave-like rapid propagation of the combustion front ensures that supersaturation is reached only at the combustion front and that nucleating particles are isolated, thus limiting crystallite growth.

The synthesis parameters required for the formation of $SrZr_{0.95}Y_{0.05}O_{3-x}$ powders are 1) (GA)/Y molar ratios greater than 3 and (GA)/Zr molar ratios greater than 2 in order to form the soluble glycolate complexes and prevent the precipitation of hydroxides and 2) pH values between 5–10 in order to form soluble complexes. The (GA)/nitrate ratio can be used to vary the temperature of the combustion. The loss of metal cations as organic complexes for higher (GA)/nitrate ratios, however, suggests that ratios near stoichiometric or lower are preferable such that higher percentages of the theoretical powder yield are obtained.

Comparison to co-precipitated powders showed that ammonium glycolate synthesized powders have better densification characteristics. The use of powder combustion synthesis methods will aid in the development of thinner membranes to increase transport rates

[25] demonstrating the advantage of using combustion methods to synthesize the precursor powders for the preparation of dense and strong membranes.

References

1. T. YAJIMA, H. SUZUKI, T. YOGO and H. IWAHARA, *Solid State Ionics* **51** (1992) 101.
2. S. HAMAKAWA, T. HIBINO and H. IWAHARA, *J Electrochem Soc* **141** (1994) 1720.
3. H. IWAHARA, H. UCHIDA and S. TANAKA, *J Appl Electr* **19** (1989) 448.
4. I. KOSACKI and H. U. ANDERSON, *Solid State Ionics* **97** (1997) 429.
5. R. W. BORRY, E. C. LU, Y.-H. KIM and E. IGLESIA, "Studies in Surface Science and Catalysis, Vol. 119" (Elsevier Science) (1998) 403.
6. J. LANGGUTH, R. DITTMEYER, H. HOFMANN and G. TOMANDL, *Appl Catal A* **158** (1997) 287.
7. T. TERAI, X. LI, K. TOMISHIGE and K. FUJIMOTO, *Chem Lett* **4** (1999) 323.
8. R. M. GERMAN, "Sintering Theory and Practice" (John Wiley & Sons, Inc., New York, 1966).
9. M. P. PECHINI, U.S.A. Patent # 3,330,687 (1967).
10. P. COURTY and B. DELMON, *Compt Rend Acad Sci C* (1969) 1874.
11. L. A. CHICK, I. R. PEDERSON, G. D. MAUPIN, J. L. BATES, L. E. THOMAS and G. J. EXARHOS, *Mater Letters* **10** (1990) 6.

12. S. S. MANOHARAN and K. C. PATIL, *J Am Ceram Soc* **75** (1992) 1012.

13. H.-C. SHIN, K.-R. LEE, S. PARK, C.-H. JUNG and S.-J. KIM, *Jpn J Appl Phys* **35** (1996) L 996.

14. L. R. PEDERSON, G. D. MAUPIN, W. J. WEBER, D. J. MCREADY and R. W. STEPHENS, *Mater Lett* **10** (1991) 437.

15. D. A. FUMO, J. R. JURADO, A. M. SEGADAES and J. R. FRADE, *Mater Res Bull* **32** (1997) 1459.

16. K. R. VENKATAKARI, D. HUANG, S. P. OSTRANDER and W. A. SCHULZE, *J Mater Res* **10** (1995) 748.

17. A. E. MARTELL and M. CALVIN, "Chemistry of the Metal Chelate Compounds" (Prentice-Hall, Inc., Englewood Cliffs, N.J., 1952).

18. K. NAKAMOTO, P. J. MCCARTHY and B. MINIATAS, *Spectrochim Acta* **21** (1965) 379.

19. J. D. S. GOULDEN, *ibid.* **16** (1960) 715.

20. R. LARSSON, *Acta Chem Scand* **19** (1965) 783.

21. J. J. KINGSLEY and L. R. PEDERSON, *Mater Letters* **18** (1993) 89.

22. T. A. RING, "Fundamentals of Ceramic Powder Processing and Synthesis" (Academic Press, San Diego, 1996).

23. M.N. RAHAMAN, "Ceramic Processing and Sintering" (Marcel Dekker, Inc., New York, 1995).

24. A. E. NIELSEN, "Kinetics of Precipitation" (Macmillan, New York, 1964).

25. E. C. LU, A. LI, L. LI and E. IGLESIA, unpublished results.